Tang, C., Yang, H., Pancost, R., Griffiths, M. L., Xiao1, G., Dang, X., & Xie, S. (2017). Tropical and high latitude forcing of enhanced megadroughts in Northern China during the last four terminations. *Earth and Planetary Science Letters*, *479*, 98-107. https://doi.org/10.1016/j.epsl.2017.09.012

Tropical and high latitude forcing of enhanced megadroughts in Northern China during the last four terminations

Changyan Tang[1, #], Huan Yang[1, #], Richard D. Pancost[2], Michael L. Griffiths[3], Guoqiao Xiao[1], Xinyue Dang[1], Shucheng Xie[1, *]

[1] *State Key Laboratory of Biogeology and Environmental Geology, School of Earth Sciences, China University of Geosciences, Wuhan 430074, China*

[2] *Organic Geochemistry Unit, Bristol Biogeochemistry Research Centre and The Cabot Institute, School of Chemistry, University of Bristol, Cantock's Close, Bristol BS8 1TS, UK*

[3] *Department of Environmental Science, William Paterson University, Wayne, NJ 07470, USA*

[#] Equal contribution

* To whom correspondence should be addressed, xiecug@163.com

ABSTRACT

Understanding the origin and evolutionary history of drought events is of great significance, providing critical insight into future hydrological conditions under the changing climate. Due to the scarcity of drought proxies from northern China, the occurrence and underlying mechanisms of the drought events remains enigmatic on longer timescales. Here we utilize microbial lipid proxies to reconstruct significant drought events over the last four ice age terminations in the southernmost section (Weinan section) of the Chinese Loess Plateau. The abundance of archaeal isoprenoid GDGTs (glycerol dialkyl glycerol tetraethers) relative to bacterial branched GDGTs, measured by $R_{i/b}$ and BIT indices, is diagnostic of enhanced drought conditions. The $R_{i/b}$ (and BIT) indices are stable and low (high) throughout most of the loess section spanning the last 350 thousand years, but they do exhibit sharp transient peaks (valleys) during the intervals associated with the four ice age terminations, and especially Terminations II and IV. These enhanced drought events are, non-intuitively, associated with a significant decrease in the relative abundance of C4 plants, inferred by a decrease in the carbon isotope composition of bulk organic matter. Although the microbial records show some consistency with the Weinan grain size profiles, indicative of Eastern

Asian winter monsoon variability, they also show some apparent difference. In fact, some features of the microbial records exhibit strong similarities with marine sediment planktonic foraminiferal $\delta^{13}C$ records from the western Pacific warm pool, which reflect ENSO-like changes during glacial terminations. Therefore, enhanced droughts immediately before the interglacial warming in northern China could be explained, at least in part, by teleconnections in tropical ocean-atmosphere circulation via shifts in the Intertropical Convergence Zone (ITCZ) and associated Jet Stream over the Asian continent. According to our microbial biomarker data, these enhanced megadroughts are apparently different, both in terms of severity and causal mechanism, from the more commonly discussed dry conditions observed during glacial periods.

Keyword: drought; microbial biomarkers; glacial terminations; Asian monsoon

Highlights

- Microbial tetraether lipids analyzed for ~350-kyr interval in Chinese Loess Plateau
- Megadroughts identified during four glacial terminations on the basis of microbial lipids
- Tropical and high latitude forcing proposed for enhanced droughts in North China
- Megadroughts during glacial terminations different from regular glacial droughts

1. INTRODUCTION

Drought events exert severe impacts on both terrestrial and aquatic ecosystems, and also society (Webster et al., 1998; Cohen et al., 2007). The history of droughts in the Asian interior has been the focus of much investigation, especially with respect to the impact of the Tibetan Plateau (TP) uplift on enhanced aridity during the late Cenozoic (Manabe et al., 1990; An et al., 2001). Indeed, grain size analyses of Chinese Loess Plateau (CLP) sediments—a proxy for the strength of East Asian winter monsoon (EAWM) winds (e.g., Ding et al., 1995)—has revealed periods of desertification in Central Asia going as far back as the Neogene (Guo et al., 2002). More recently, speleothem records from central (e.g., Wang et al., 2008; Cheng et al., 2009, 2016) and southwest (e.g., Cai et al., 2015) China have shown, via oxygen-isotope ratios ($\delta^{18}O$) [proxy of Asian summer monsoon (ASM) variability], precession-driven fluctuations in the ASM through glacial-interglacial cycles, as well as millennial-scale perturbations during the last glacial-deglaciation apparently driven by North Atlantic (e.g. Wang et al., 2008) and Antarctic (e.g., Zhang et al., 2016) meltwater events. Records from the western CLP have shown that glacial boundary conditions (i.e. sea ice, atmospheric CO_2) have a more dominant influence on summer precipitation changes in North China (Sun et al., 2015).

Despite these advancements in our understanding of orbital- and millennial-scale ASM variability, there still remains a large gap in our knowledge of the spatial homogeneity (or heterogeneity) of monsoon variability in China under varying boundary conditions, and in particular, how changes in the summer monsoon can be manifested as periods of enhanced drought. This is because hitherto most of the longer-term terrestrial monsoon records are sourced from the $\delta^{18}O$ of the ever-growing speleothem network, despite recent research suggesting that these proxies, particularly those located over central China, primarily reflect large-scale Indian Summer Monsoon (ISM) variability upstream of the cave sites, and not necessarily local precipitation amount (e.g., Pausata et al., 2011; Liu et al., 2014). Therefore, we still lack longer-term records of enhanced drought conditions, or 'megadroughts', from the ASM domain, particularly in the CLP region. Recent work by Cook et al. (2010) identified a series of megadroughts [i.e. extreme hydrological events of naturally occurring multidecadal precipitation variations (Meehl et al., 2006)] over the last millennium, which were attributed to summer monsoon failures associated with tropical Pacific sea surface temperature (SST) anomalies. Moreover, Zhang et al. (2008) showed that prolonged periods of monsoon failure occurred over the past millennium, and interestingly, linked these megadrought events with the demise of several Chinese dynasties. Despite these studies shedding light on the magnitude and frequency of these megadroughts in East Asia, their relative brevity precludes a robust assessment of these extreme events on longer time scales (i.e. glacial-interglacial, G-IG time scales). In addition, whilst there are records from the western (e.g., Sun et al., 2006, 2015) and northern CLP (Guo et al., 2009; Hao et al., 2012) which suggest that dry conditions prevailed during glacial times, we still know very little about how the southern sector of the plateau responded to high and low latitude forcing. Hence, gaining a deeper insight into the occurrence of these enhanced megadrought conditions at this location is critical given the importance of monsoon precipitation to the agriculture of the region.

In contrast to paleotemperature reconstructions, records of past aridity, particularly on geologic timescales, are especially difficult to obtain given the lack of reliable and well preserved proxies. Glycerol Dialkyl Glycerol Tetraethers (GDGTs, Fig. S1), which are membrane lipids synthesized by archaea and bacteria (Schouten et al., 2013), have been used to reconstruct the paleoclimate history of the CLP, particularly paleotemperature (Gao et al., 2012; Jia et al., 2013; Peterse et al., 2011, 2014; Yang et al., 2014; Thomas et al., 2016). However, in addition to soil alkalinity (Xie et al., 2012; Yang et al., 2014), recent research has shown that the distributions of archaeal isoprenoid GDGTs (iGDGTs) and bacterial branched GDGTs (brGDGTs) are also influenced by soil moisture (Wang et al., 2013; Dirghangi et al., 2013). Most notably, the $R_{i/b}$ ratio (i.e. the abundance of total iGDGTs relative to total brGDGTs) has been shown to significantly increase during extreme arid conditions, and as such, has the potential to be a reliable terrestrial archive of enhanced droughts (Xie et al., 2012). In this study, we show that elevated $R_{i/b}$ values (>0.5) in the southern sector [Weinan section (WS)] of the CLP likely mark intervals of enhanced drought, defined as periods where mean annual precipitation (MAP) is less than 600 mm (Yang et al., 2014, supplemental data Fig. S2). The 'enhanced drought' term is used here to discriminate from 'regular drought' conditions identified during glacial periods. The term 'megadrought' is further used to identify enhanced drought conditions (identified by the $R_{i/b}$ ratio) that occurred over long periods of time (e.g., over multiple decades; Meehl et al., 2006). Furthermore, through a survey of the relationship between $R_{i/b}$ values and soil moisture (ranging from 0 to 61%) along three transects perpendicular to the shoreline of Qinghai Lake (located in the transitional zone between the TP and Chinese Loess Plateau), we find that $R_{i/b}$ values markedly increase when soil water drops below 30% (Dang et al., 2016), corroborating the reliability of $R_{i/b}$ as an indicator of enhanced drought (supplemental data, Fig. S3).

A closely related GDGT-based proxy, the BIT (Branched and Isoprenoid Tetraethers) index, estimates the relative abundance of the main brGDGTs (brGDGTs-I, -II, -III) vs. one specific iGDGT, crenarchaeol, which is biosynthesized by a group of archaea (Thaumarchaeota). Initially, the BIT index was proposed to evaluate the input of terrestrial organic material into immature marine and lake sediments (Hopmans et al., 2004), although later it was found to exhibit a relationship with mean annual precipitation (Dirghangi et al., 2013) and water content (Wang et al., 2013) in soils. In light of these findings, there is strong potential for BIT to be a robust humidity proxy in terrestrial settings (supplemental data, Fig. S2). Our results show an inverse relationship between $R_{i/b}$ and the BIT index, though it is worth noting that the range of $R_{i/b}$ values is much larger when BIT values become relatively low, indicating the potential tandem utility of these proxies in identifying enhanced drought events (Yang et al., 2014). Therefore, we utilized both of these novel soil moisture proxies to identify periods of enhanced aridity in the monsoon-dominated region of the CLP over the past 350,000 years. Our findings will add to the growing body of records derived from loess-paleosol sequences of the CLP for the Quaternary (e.g., An et al., 2001), providing critical new information on past variations in monsoon climate, and the strong links with Earth's changing boundary conditions (e.g., pCO_2, sea level, insolation).

2. STUDY SITE AND METHODS

2.1. *Study site and sampling*

The loess sequence from Weinan is located at the southern tip of the CLP (34°21.0′ N; 109°32.0′E), and marks one of the wettest areas of the plateau (Fig.1a). The mean annual air temperature (MAAT) at Weinan is 13.8°C and the mean annual precipitation (MAP) is 570 mm (based on China Meteorological Administration climate records during 1981-2010, http://www.cma.gov.cn). The modern climate at the site is highly seasonal, with temperatures typically exceeding 20°C between May and September and typically lower than ~5°C between November and January. The annual rainfall is also highly seasonal and largely governed by the strength of the East Asian summer monsoon (EASM), with 70% of the annual precipitation delivered between May and September by moisture-laden air masses sourced from the tropical oceans (Fig. 1c). The end of the EASM season is marked by a shift in wind direction as the East Asian winter monsoon winds from the west bring cold and dry conditions to the region.

The Weinan section investigated here contains 34.8 m of loess-paleosol (LPS), extending from the L_4LL_1 loess [the topmost of L_4 phase corresponding to Marine Isotope Stage (MIS) 10] to the Holocene paleosol S_0, covering the last three glacial-interglacial cycles (MIS1-9). The samples were collected at 10cm intervals.

2.2. *Grain size and magnetic susceptibility analysis*

The magnetic susceptibility (χ) and sediment grain size were analyzed on samples extracted at 10 cm intervals. The magnetic susceptibility and grain size analyses were conducted following the methods of Hao et al. (2012). Specifically, the low-frequency analysis of χ (n=349 samples) was measured at 0.47 kHz using a Bartington Instruments MS 2B magnetic susceptibility meter. For grain size analysis, the samples were treated with 10% H_2O_2 and 10% HCl solution to remove organic matter and carbonate, respectively. After dispersal using 0.05 mol/L $(NaPO_3)_6$, the samples were measured using a Mastersizer 2000 analyzer with the range of 0.02-2,000 μm in diameter, and a precision of ±1%.

2.3. *Age model*

The age model of the Weinan section was obtained by interpolation between geomagnetic polarity boundaries (Ding et al., 2002), using χ as an indicator of accumulation rate (Ding et al., 2002; Kukla et al., 1988). This model is widely used to date the loess-paleosol sections of the CLP. The χ and grain size data, analyzed at 10 cm intervals, represent an average time resolution of 0.3-2.6 kyr.

2.4. *Lipid extraction*

A total of 198 loess-paleosol samples were transported to the lab immediately after collection, and dried in an oven at 45°C. The samples were ground into powder with a mortar and pestle, and passed through a 20-mesh sieve (0.85 mm in diameter) to remove tiny roots and carbonate nodules. An aliquot of each sample (40-50g) was extracted with dichloromethane (DCM): methanol (9:1, v/v) using an accelerated solvent extractor (ASE 100, Dionex, USA) at 100°C and 1400psi. The total lipid extracts were concentrated by a rotary evaporator and separated into apolar and polar fractions using flash silica gel column (0.7 cm i.d. and 1.5g activated silica gel) chromatography and with hexane (10ml) and methanol (10ml) as the eluents, respectively. All polar fractions containing GDGTs were passed through 0.45μm PTFE syringe filters and dried under nitrogen gas. The 198 samples for GDGT analysis in this study include 37 samples of the S_0 layer reported by Yang et al. (2014).

2.5. *GDGT analysis and proxy calculation*

Each polar fraction was re-dissolved in 300 μl *n*-hexane: ethyl acetate (EtOA) (84:16, v/v), and a C_{46} GDGT was added as a synthesized internal standard. 15μl of each sample were injected and analyzed by an Agilent 1200 series liquid chromatography coupled to an Agilent 6460A triple quadruple mass spectrometer (LC-MS/MS). Separation of the brGDGTs was performed on two silica columns (150mm×2.1mm, 1.9μm, Thermo Finnigan) in tandem. The elution gradients were matched following the description of Yang et al. (2015). The single ion monitoring (SIM) was used, monitoring at *m/z* 1302, 1300, 1298, 1296, 1292, 1050, 1048, 1046, 1036, 1034, 1032, 1022, 1020, 1018 and 744. The 5- and 6-methyl brGDGTs were identified by the relative time order of compound peaks. Compound quantification was performed by peak area integration of $[M+H]^+$ in the extracted ion chromatogram. MS conditions follow Hopmans et al. (2004). The 6-metylated brGDGTs are identified by an accent after the roman numerals for their corresponding 5-methylated isomers. The typical analytical errors for $R_{i/b}$ and BIT are all better than 0.02.

The $R_{i/b}$ proxy was used to identify enhanced aridity conditions (Xie et al., 2012) and calculated as follows:

$$R_{i/b} = \sum(\text{iGDGTs}) / \sum(\text{brGDGTs})$$

BIT is calculated according to the following formula (Hopmans et al., 2004):

$$BIT = (Ia + IIa + IIa' + IIIa + IIIa') / (Ia + IIa + IIa' + IIIa + IIIa' + \text{crenarchaeol})$$

where Roman Numerals indicate the molecular structures of GDGTs shown in supplemental data (Fig. S1).

2.6. Spectral analysis

The Arand software package (Howell et al., 2006) was used to calculate power spectra and phase of time series. The spectral density of magnetic susceptibility and $R_{i/b}$ was analysed at 1 ka interval after all the data were detrended. The Analyseries software was used to conduct f-tests of spectral peak significance (Paillard et al., 1996).

3. RESULTS AND DISSCUSION

3.1. Distribution of GDGTs in the Weinan loess section

Both iGDGTs and brGDGTs were detected in all samples. The concentrations of GDGTs are higher in paleosol layers than in adjacent loess layers. In most samples, brGDGTs accounted for a higher proportion of total GDGTs (84.8% in average). Crenarchaeol is the most abundant iGDGT. GDGT-Ia, -Ib, and -IIa' are the most abundant of the brGDGTs and constitute almost 70% of the total brGDGTs on average. The GDGT-IIIc has the lowest concentration in nearly all samples, and is below the detection limit in some cases. The average distribution of GDGTs in loess layers was not significantly different from the paleosols.

It is noteworthy that the 6-methyl brGDGTs constitute, on average, 32.9% of the total brGDGTs, which has implications for mean annual air temperature reconstruction (see below). Similarly, the proportion of brGDGT-IIa, one of the main components in brGDGT-based proxies, is lower in the Weinan loess (0.7%-9.6%, 3.6% on average) than in the global soils dataset (0%-24%, 18% on average).

3.2. *Paleotemperature reconstruction of the Weinan section*

In combination with the widely-used age models of the CLP (e.g., Kukla et al., 1988; Porter and An, 1995), paleotemperature records reconstructed from the molecular proxies in the same section, could potentially help to further constrain the timing of glacial terminations in northern China. Indeed, branched GDGTs have been used to reconstruct the MAAT at various locations across the planet, usually based on global MBT (methylation index of branched tetraethers) and CBT (cyclization of branched tetraethers) indices against MAAT and pH (as initially proposed by Weijers et al., 2007, and later refined by Peterse et al., 2012). It is noteworthy that MAATs derived from the global MBT/CBT calibrations are typically too high when applied to arid regions, including the CLP (Gao et al., 2012; Jia et al., 2013; Peterse et al., 2014; Peterse et al., 2011; Dang et al., 2016). However, the relatively new global calibration based primarily on the 5-methylated and tetramethylated brGDGTs appears to minimise the influence of precipitation and to reduce the error in paleotemperature reconstruction in the semi-arid and arid regions (De Jonge et al.,2014):

$$MATmr= 7.17 + 17.1\times[Ia] + 25.9\times[Ib]+ 34.4\times[Ic]-28.6\times[IIa]$$

where roman numerals correspond to the molecular structures of GDGTs shown in the supplemental Fig. S1.

Over the last 350 ka, the WS shows large variations (~10.6 °C range) in MAAT on glacial-interglacial timescales (Fig. 3h). The reconstructed MAAT exhibits a maximum of 23.7 °C at the beginning of MIS7 (ca. 250 ka BP), which is slightly warmer than MIS 5 (ca. 130 ka BP). This result is somewhat surprising given that MIS5 is generally thought to represent the globally warmest interglacial period of the studied interval. The brGDGT-derived MAAT record also reveals that MIS 5c (ca. 113 ka B.P.) was the warmest within MIS5. This is similar to the results of Lu et al. (2007) and Peterse et al. (2014), also based on brGDGT distributions. As expected, the lowest reconstructed MAATs occur during glacial times (Fig. 3h), with the temporal patterns showing broad similarities to other records. During terminations I, II, III and IV, the MAAT at our site exhibits minimum values. Not surprisingly, these periods of minimum MAATs in the southern CLP coincide with low NH summer insolation (Fig. 3l). Conversely, periods of warming are matched by higher summer insolation. The strong connections between Weinan MAAT and both global ice volume and

NH summer insolation highlight the sensitivity of the region to shifts in Earth's boundary conditions. As discussed in more detail below, in most cases the dramatic drop in reconstructed MAATs is associated with very low BIT values (Fig. 3g) and high $R_{i/b}$ ratios (Fig. 3f), lending support to the conclusion that the enhanced drought events occurred during glacial terminations in the CLP. It is worth noting, however, that there are several sudden declines in temperature that do not correspond to changes in BIT and $R_{i/b}$, such as during precession minima through MIS4 and MIS6. The cold climate in the CLP was thus not necessarily accompanied by the occurrence of extreme drought events.

3.3. Molecular and sedimentological records of intensified drought events

Our microbial lipid record (n=198 samples) indicates that the $R_{i/b}$ ratio remains relatively low and stable throughout most of the record (Fig. 3f). It is reasonable to assume that the $R_{i/b}$ ratios did not change when the precipitation was >600 mm or the soil water content was > 30% (Fig. S3), such that intervals with low ratios could have still experienced mildly arid conditions. The exceptions to this overall stability are the very large and abrupt increases that occur during the transitional periods from loess to paleosol (i.e., from L_2 to S_1, L_3 to S_2, and L_4 to S_3) (Fig. 3). These intervals correspond with the glacial terminations, including Terminations II-IV (Fig. 3f), where values increased 5-15 fold when local MAAT was ~14-16 °C (Fig. 3f). Specifically, $R_{i/b}$ ratios increase from a baseline value of ~0.2 [typical for soils from non-arid settings (Yang et al., 2014)] to a ratio of ~0.5 during Terminations III and IIIa which is typically characteristic of soils with a pH > 8 (Yang et al., 2014); values were highest during Terminations II and IV where ratios exceeded 0.83. An increase in $R_{i/b}$ ratios (0.40), albeit smaller than that observed during the other terminations (0.40), also occurs at the L_1/S_0 boundary corresponding to the T-I. However, the relatively lower values through T-I, compared with other terminations, merits further investigation. Remarkably, besides the terminations, the only time the $R_{i/b}$ ratios exceed a value 1 is during the late Holocene, which is probably due to land use changes. For example, agricultural practices can lead to the surface soils becoming more loose and porous, and as a result, the ability of the soil to hold water decreases and the evaporation potential increases, ultimately drying out the surface soils.

Additional evidence for the increased $R_{i/b}$ ratios reflecting drought conditions is provided by the WS BIT indices, which range from 0.38 to 0.98 and exhibit the same trends as the $R_{i/b}$ values throughout the whole sequence. Although the BIT index is also a ratio of isoprenoidal and branched GDGTs, it comprises different GDGTs and therefore different microorganisms, providing additional evidence for profound change in the microbial community.

The large changes in $R_{i/b}$ ratios (and BIT indices) provide direct evidence for a more arid North China climate during glacial terminations. It is notable though that the microbial proxies presented here only record very enhanced drought, or megadroughts, but not the more subtle drought events (Xie et al., 2012). Hence, this likely explains the differences between our records and those proxies [e.g. grain size (Ding et al., 2002; Hao et al., 2012) and WSχ□ (An et al., 1991)] that are associated with more subtle changes in the monsoon system. Our results are in-line with previous findings from the region (e.g., Guo et al., 2009; Hao et al., 2012), suggesting that megadroughts occurred during glacial terminations, when NH ice volume was greatest and NHSI (North Hemisphere Summer Insolation) was generally low (Fig. 4). Moreover, our record likely explains previously reported sedimentological features in central Asia, including the extremely high accumulation rate of loess in the west Kunlun area of the TP (Zan, 2010), the absence of growth intervals in Kesang cave stalagmite records from the western TP (Cheng et al., 2012), and the low values in loess deposits from Jingyuan (Sun et al., 2006) and Chashmanigar, Tajikistan (Ding et al., 2002).

The inferred shifts in megadroughts at Weinan (inferred from the BIT and $R_{i/b}$ records) are concentrated at the glacial-interglacial timescale (100-kyr scale) (Fig. 5), whereas the occurrence of pluvials and droughts are also modulated by Earth's precessional cycle, akin to the signals preserved in Chinese speleothem records from Hulu and Sanbao caves (Wang et al., 2008; Cheng et al., 2009, 2016). Indeed, higher (lower) speleothem $\delta^{18}O$ values, indicative of a weaker (stronger) Indian summer monsoon (e.g., Pausata et al., 2011; Liu et al., 2014), are matched by intervals of lower (higher) WS χ and higher (lower) WS grain size values, suggesting weaker (stronger) EASM and stronger (weaker) EAWM conditions, respectively, during periods of low (high) NHSI. This result suggests that the high $R_{i/b}$ values primarily reflect only the most severe drought events, associated with glacial terminations.

The extremely cool and dry conditions during glacial terminations would also have impacts on the vegetation of the CLP. Evidence for this comes from □^{13}C-depleted bulk soil organic matter which indicates, unexpectedly, a sudden decrease in the relative abundance of C4 plants in the Weinan loess-paleosol sequence (Fig. 3c) (Sun et al., 2011). Large $\delta^{13}C$ variations have been used to estimate shifts in the C3/C4 ratio of vegetation because of the different photosynthetic pathways associated with these plant types (O'Leary, 1988). Whilst some studies have interpreted the $\delta^{13}C$ changes in loess-paleosol sequences to reflect shifts in water use efficiency and aridity (Hatte and Guiot, 2005; Zech et al., 2007), others have proposed that the vegetation changes are primarily governed by temperature. For example, several studies have proposed that cold (warm) climates were characterized by a general expansion (reduction) of C3 (C4) vegetation in the CLP (Zhang et al., 2003; Liu et al., 2005). The consistency between enhanced drought conditions and negative $\delta^{13}C$ excursions during glacial times contradicts what is expected for an aridity control, and thus favours the latter interpretation.

3.4. Mechanism for enhanced aridity during glacial terminations

The enhanced drought events identified by the $R_{i/b}$ and BIT proxies during glacial terminations are generally associated with an higher percentage of grain size > 32μm, diagnostic of the intensification of EAWM (An et al., 1991; Ding et al., 2002; Hao et al., 2012). Moreover, the episodic droughts identified by WS — i.e. the monsoon failures typically occurring during periods of reduced NHSI — are coeval with higher WS grain size. Therefore, it is likely that periods of summer monsoon failure were strongly linked with the synchronous increases in winter monsoon winds, which are known to influence hydroclimate in China on G-IG time scales via shifts in the ITCZ (e.g., Yancheva et al., 2007; Cosford et al., 2008); a stronger winter monsoon would push the ITCZ and the rain belt southwards, resulting in increased aridity in northern China. However, there are some apparent differences between the EASM and EAWM proxies (Fig. 3i, j), suggesting that changes in the EAWM cannot fully explain the observed enhanced droughts during glacial terminations.

Comparison between the reconstructed southern CLP megadroughts presented here reveal, to an extent, similarities with ice-rafted debris (IRD) records from the North Atlantic (Fig. 3e). The two major $R_{i/b}$ maxima during T-II and T-IV are coincident with significant increases in IRD. The relatively smaller $R_{i/b}$ increases during T-III are associated with similarly small increases in IRD. Previous work has illustrated the strong influence of North Atlantic meltwater pulses (i.e. Heinrich events) on northern China aridity (e.g., Guo et al., 1996). An increased freshwater flux to the North Atlantic during the last deglaciation, associated with enhanced IRD deposition, would have resulted in a slow-down of the Atlantic meridional overturning circulation (AMOC) (e.g., McManus et al., 2004; Böhm et al., 2014). The climate signal of the North Atlantic appears to have been transmitted to the Asian monsoon regions via the northern westerlies, leading to enhanced EAWM winds and reduced summer monsoon precipitation (Sun et al., 2012). However, not all the IRD events are associated with enhanced drought in northern China. For example, the maximum IRD event at ~280 ka BP, corresponding to loess deposition during mid L_3, exhibits no association with both the WS BIT and $R_{i/b}$ indices, and hence no enhanced drought event. In addition, the generally high IRD deposition between 75 and 25 ka BP, corresponding to the loess deposition L_1, is also not matched by anomalous BIT and $R_{i/b}$ values, at least when compared with those events occurring at T-II and T-IV. Thus, we conclude that although North Atlantic freshwater influx events could have brought about CLP enhanced drought, other teleconnections with the NH were also important.

The simulations of Sun et al. (2015) and others (e.g., Kutzbach and Guetter, 1986; Kutzbach et al., 2008; Weber and Tuenter, 2011; Lu et al., 2013; Liu et al., 2014), suggest that the dominant forcings imposed on the mid latitude monsoon regions are changing surface boundary conditions (ice sheet extent, sea ice, land albedo), whereas monsoon regions closer to the equator appear to be more influenced by summer insolation. This is certainly apparent in the WS record, along with those of Sun et al. (2015, Fig. 5b), which show a dominant 100-kyr signal, whereas the speleothem records from southern China show a dominant precessional (23-kyr) signal (Fig. 5a). Of particular note, the model sensitivity experiments conducted by Sun et al. (2015) demonstrate that the spatial variability is primarily the result of the southern monsoon regions, particularly those sites located near the coast, being dominated by changes in the land-sea thermal contrast, which is modulated by summer insolation (Kutzbach and Guetter, 1986). By contrast, the more northern sites in China are more influenced by the shifting westerlies, and their interaction with the Tibetan Plateau (e.g., Chiang et al., 2014). Specifically, empirical evidence has shown that increased NH ice sheet extent, such as during glacial maximums, likely increased the hemispheric thermal gradient (NH hemisphere cooler than the SH) (Yanase and Abe-Ouchi, 2007; Jiang et al., 2011), which lead to an increase in the westerlies (e.g., Yanase and Abe-Ouchi, 2007) and therefore strengthened EAWM winds. In addition, the extent of the NH ice sheets also pushes the Siberian High further southwards, which consequently acts to block the northward migration of the Asian Summer monsoon (Peterse et al., 2014; Thomas et al., 2017). At the same time, sea level was lower as was atmospheric CO_2 concentrations. Model simulations suggest that all of these factors could have contributed to preventing the monsoon front from penetrating as far north as the CLP, thus reducing summer monsoon rainfall amount in Northern China (Sun et al., 2015). Whilst the effects of insolation, ice sheet extent, and CO_2 impact all of East Asia, the magnitude of these forcings on the hydroclimate varies from south to north. For example, the model simulations indicate that the magnitude of monsoon reductions induced by increased ice and decreased CO_2 (such as during the LGM), are much greater in Northern China compared with Southern China (Sun et al., 2015).

Despite the model simulations described above suggesting that changing glacial-interglacial boundary conditions (e.g., ice sheets, land albedo, and sea ice) impose a greater forcing on mid latitude monsoons than local and/or tropical forcing (e.g., insolation), it is unlikely that the effects of ice volume alone can explain the observed enhanced droughts in the CLP. This is because these effects should be similarly impactful during glacial periods, but they are only observed during terminations. Therefore, other forcing factors must play a role in amplifying the response from NH ice sheet extent. To that end, we find evidence for extreme droughts also being linked with variations in the tropical oceans. In particular, the enhanced aridity records reconstructed here (via molecular proxies) are consistent with *P. obliquiloculata* stable carbon isotope minima from the western Pacific warm pool (WPWP; Fig. 3d, Jia et al., 2015). The two major $R_{i/b}$ maxima during T-II and T-IV, are associated with the two largest decreases in $\delta^{13}C$ values in the WPWP of the past 350 thousand years. Moreover, the relatively smaller $R_{i/b}$ increases during T-III are associated with similarly small decreases in $\delta^{13}C$. These phase relationships suggest that, in addition to high northern latitude forcings, the threshold of megadroughts in Northern China could also be connected with changes occurring in the tropical Pacific.

The $\delta^{13}C$ values of planktic subsurface water species *P. obliquiloculata* in the western Pacific MD06-3047B core (Fig. 3d) show highly depleted excursions during T-I, T-II, and T-IV. During terminations, these $\delta^{13}C$ data suggest that the thermocline was lower in the WPWP compared with the Eastern Pacific (Jia et al., 2015; Farrell et al., 1995), similar to El-Niño conditions today. This teleconnection pattern is proposed to have induced changes in El Niño-Southern Oscillation (ENSO)-like variability, comprising a complicated high- and low-latitude feedback mechanism during glacial terminations (Pena et al., 2008). These meridional teleconnections travel through the atmosphere via latitudinal shifts in wind patterns and through the ocean by circulation changes of intermediate water from the polar regions to the tropical thermocline waters (Pena et al., 2008). Model-proxy syntheses have also suggested an altered ENSO state during the LGM via the first-order influence of the exposed Sunda Shelf landmass on the Walker circulation (DiNezio and Tierney, 2013). Specifically, the models and proxy records highlighted in their study suggest that the exposed Sunda and Sahel Shelves drove reductions in convection over the Indo-Pacific during glacial terminations. Moreover, speleothem $\delta^{18}O$ records from Borneo (e.g., Meckler et al., 2012; Carolin et al., 2016), which show decreased convection during T-I (and other terminations), appear to align with this Walker circulation mechanism, although as pointed out by Carolin et al. (2013), the timing of Sunda Shelf inundation during T-I and T-II relative to Borneo $\delta^{18}O$ changes are not consistent between the terminations (Fig. 3b). Regardless of the mechanism driving the reduced convection over the Indo-Pacific warm pool (IPWP), it appears that on G-IG time scales, reduced convection in this region during glacial terminations played a critical role in amplifying megadrought conditions over the CLP, possibly due to a reduction in atmospheric heat and vapor transport from the tropics. Under modern conditions, reduced convection over the IPWP, for example during El Niño years, leads to an overall decrease in precipitation over Northern China (Xiao et al., 2000; Gong and Wang, 1999), and thus has led to enhanced droughts in the Northern Chinese Plains (Huang and Wu, 1989). Because the ITCZ tends to be constrained closer to the equator during El Niño events, an equatorward ITCZ shift in East Asia would lead to a moisture deficit in Northern China.

4. CONCLUSIONS

We identify enhanced drought events at the last four ice age terminations on the basis of microbial lipid distributions in the southernmost part (Weinan section) of the Chinese Loess Plateau. The abundance of archaeal isoprenoid GDGTs (glycerol dialkyl glycerol tetraethers) relative to bacterial branched GDGTs, measured by $R_{i/b}$ and BIT indices, is diagnostic of extreme drought events. The $R_{i/b}$ (and BIT) indices are stable and low (high) throughout most of the loess section spanning the last 350 thousand years, but they exhibit sharp transient peaks (valleys) during the intervals corresponding to the four ice age terminations, and especially those of Termination II and IV. These enhanced drought events occurring immediately before the interglacial warmings are different from, but much more severe than, the dry conditions during glacial periods. These enhanced megadroughts appear to be controlled by changing glacial-interglacial boundary conditions (e.g., ice sheets, land albedo, and sea ice) affecting the position of westerlies, but also amplified by a reduction in northward heat/moisture transport from the IPWP because of cooler SSTs and a weaker Walker circulation during glacial terminations.

ACKNOWLEDGMENTS

We thank He G., Liu H., Ma L., and Gao Q for field sampling, and Ding W. for assistance in the lipid analysis. We also thank Zhang H. for valuable advice on an early version of this paper. This work was supported by National Natural Science Foundation of China (Grant No., 41330103), State Key R&D project (Grant No., 2016YFA0601100) and the 111 program (Grant No., B08030). RDP acknowledges the Royal Society Wolfson Research Merit Award and the ERC Advanced Grant T-GRES.

REFERENCES CITED

An, Z., Colman, S.M., Zhou, W., Li, X., Brown, E.T., Jull, A.T., Cai, Y., Huang, Y., Lu, X., Chang, H., 2012. Interplay between the Westerlies and Asian monsoon recorded in Lake Qinghai sediments since 32 ka. Sci. Rep-UK 2, 619.

An, Z., Kukla, G.J., Porter, S.C., Xiao, J., 1991. Magnetic susceptibility evidence of monsoon variation on the Loess Plateau of central China during the last 130,000 years. Quatern.

Res. 36, 29-36.

An, Z., Kutzbach, J.E., Prell, W.L., Porter, S.C., 2001. Evolution of Asian monsoons and phased uplift of the Himalaya–Tibetan plateau since Late Miocene times. Nature 411, 62-66.

Berger, A., Loutre, M.F., Yin, Q., 2010. Total irradiation during any time interval of the year using elliptic integrals. Quatern. Sci. Rev. 29, 1968-1982.

Böhm, E., Lippold, J., Gutjahr, M., Frank, M., Antz, B., Fohlmeister, J., Frank, N., Andersen, M. B., Deininger, M., 2014. Strong and deep Atlantic meridional overturning circulation during the last glacial cycle. Nature 517, 73-76.

Cai, Y., Fung, I.Y., Edwards, R.L., An, Z., Cheng, H., Lee, J.E., Tan, L., Shen, C.C., Wang, X., Day, J.A., 2015. Variability of stalagmite-inferred Indian monsoon precipitation over the past 252,000 y. P. Natl. Acad. Sci. USA 112, 2954-9.

Carolin, S.A., Cobb, K.M., Adkins, J.F., Clark, B., Conroy, J.L., Lejau, S., Malang, J., Tuen, A.A., 2013. Varied response of western Pacific hydrology to climate forcings over the last glacial period. Science 340, 1564-6.

Carolin, S.A., Cobb, K.M., Lynch-Stieglitz, J., Moerman, J.W., Partin, J.W., Lejau, S., Malang, J., Clark, B., Tuen, A.A., Adkins, J.F., 2016. Northern Borneo stalagmite records reveal West Pacific hydroclimate across MIS 5 and 6. Earth Planet. Sci. Lett. 439, 182-193.

Cheng, H., Edwards, R.L., Broecker, W.S., Denton, G.H., Kong, X., Wang, Y., Zhang, R., Wang, X., 2009. Ice age terminations. Science 326, 248-252.

Cheng, H., Edwards, R.L., Sinha, A., Spötl, C., Liang, Y., Chen, S., Kelly, M., Kathayat, G., Wang, X., Li, X., 2016. The Asian monsoon over the past 640,000 years and ice age terminations. Nature 534, 640-646.

Cheng, H., Zhang, P.Z., Spötl, C., Edwards, R.L., Cai, Y.J., Zhang, D.Z., Sang, W.C., Tan, M., An, Z.S., 2012. The climatic cyclicity in semiarid- arid central Asia over the past 500,000 years. Geophys. Res. Lett. 39, 1045-1062.

Chiang, J.C.H., Lee, S.Y., Putnam, A.E., Wang, X., 2014. South Pacific Split Jet, ITCZ shifts, and atmospheric North–South linkages during abrupt climate changes of the last glacial period. Earth Planet. Sci. Lett. 406, 233–246.

Cohen, A.S., Stone, J.R., Beuning, K.R., Park, L.E., Reinthal, P.N., Dettman, D., Scholz, C.A., Johnson, T.C., King, J.W., Talbot, M.R., 2007. Ecological consequences of early Late Pleistocene megadroughts in tropical Africa. P. Natl. Acad. Sci. USA 104, 16422-16427.

Cook, B. I., Smerdon, J. E., Seager, R., Cook, E.R., 2014. Pan-Continental Droughts in North America over the Last Millennium. J. Climate 27, 383-397.

Cook, E. R., Anchukaitis, K. J., Buckley, B. M., D'Arrigo R. D., Jacoby, G. C., Wright, W. E., 2010. Asian Monsoon failure and megadrought during the last millennium. Science 328, 486-489.

Cosford, J., Qing, H., Eglington, B., Mattey, D., Yuan, D., Zhang, M., Cheng, H., 2008. East Asian monsoon variability since the Mid-Holocene recorded in a high-resolution, absolute-dated aragonite speleothem from eastern China. Earth Planet. Sci. Lett. 275, 296–307.

Dang, X., Yang, H., Naafs, B.D.A., Pancost, R.D., Xie, S., 2016. Evidence of moisture control on the methylation of branched glycerol dialkyl glycerol tetraethers in semi-arid and arid soils. Geochim. Cosmochim. Acta 189, 24-36.

De Jonge, C., Hopmans, E.C., Zell, C.I., Kim, J., Schouten, S., Sinninghe Damsté, J.S., 2014. Occurrence and abundance of 6-methyl branched glycerol dialkyl glycerol tetraethers in soils: Implications for palaeoclimate reconstruction. Geochim. Cosmochim. Acta 141, 97-112.

Dinezio, P.N., Tierney, J.E., 2013. The effect of sea level on glacial Indo-Pacific climate. Nat. Geosci. 6, 485-491.

Ding, Z., Derbyshire, E., Yang, S., Yu, Z., Xiong, S., Liu, T., 2002. Stacked 2.6-Ma grain size record from the Chinese loess based on five sections and correlation with the deep-sea $\delta^{18}O$ record. Paleoceanography 17, 5-1-5-21.

Ding, Z., Ranov, V., Yang, S., Finaev, A., Han, J., Wang, G., 2002. The loess record in southern Tajikistan and correlation with Chinese loess. Earth Planet. Sci. Lett 200, 387-400.

Ding, Z., Liu, T., Rutter, N.W., Yu, Z., Guo, Z., Zhu, R., 1995. Ice-volume forcing of East Asia winter monsoon variations in the past 800,000 years. Quatern. Res. 44, 149-159.

Dirghangi, S.S., Pagani, M., Hren, M.T., Tipple, B.J., 2013. Distribution of glycerol dialkyl glycerol tetraethers in soils from two environmental transects in the USA. Org. Geochem. 59, 49-60.

Farrell, J., W., Murray, D., W., Mckenna, V., S., Ravelo A., C., 1995. Upper ocean temperature and nutrient contrasts inferred from Pleistocene planktonic foraminifer δ^{18}O and δ^{13}C in the eastern equatorial Pacific. Proceedings of the Ocean Drilling Program Scientific Results 138, 289-319.

Gao, L., Nie, J., Clemens, S., Liu, W., Sun, J., Zech, R., Huang, Y., 2012. The importance of solar insolation on the temperature variations for the past 110kyr on the Chinese Loess Plateau. Palaeogeogr. Palaeocl. 317–318, 128–133.

Gong, D., Wang, S., 1999. Impacts of ENSO on rainfall of global land and China. Chin. Sci. Bull. 44, 852-857.

Guo, Z., Berger, A., Yin, Q., Qin, L., 2009. Strong asymmetry of hemispheric climates during MIS-13 inferred from correlating China loess and Antarctica ice records. Clim. Past 5, 21-31.

Guo, Z., Liu, T., Guiot, J., Wu, N., Lü, H., Han, J., Liu, J., Gu, Z., 1996. High frequency pulses of East Asian monsoon climate in the last two glaciations: Link with the North Atlantic. Clim. Dynam. 12, 701-709.

Guo, Z., Ruddiman, W.F., Hao, Q., Wu, H., Qiao, Y., Zhu, R., Peng, S., Wei, J., Yuan, B., Liu, T., 2002. Onset of Asian desertification by 22 Myr ago inferred from loess deposits in China. Nature 416, 159-163.

Hao, Q., Wang, L., Oldfield, F., Peng, S., Qin, L., Song, Y., Xu, B., Qiao, Y., Bloemendal, J., Guo, Z., 2012. Delayed build-up of Arctic ice sheets during 400,000-year minima in insolation variability. Nature 490, 393-396.

Hatte, C., Guiot, J., 2005. Palaeoprecipitation reconstruction by inverse modelling using the isotopic signal of loess organic matter: application to the Nussloch loess sequence (Rhine Valley, Germany). Clim. Dynam. 25, 315–327.

Hopmans, E.C., Weijers, J.W., Schefuß, E., Herfort, L., Sinninghe Damsté, J.S., Schouten, S., 2004. A novel proxy for terrestrial organic matter in sediments based on branched and isoprenoid tetraether lipids. Earth Planet. Sci. Lett. 224, 107-116.

Howell, P., Pisias, N., Ballance, J., Baughman, J., Ochs, L., 2006. ARAND Time-Series Analysis Software. Brown University, Providence, RI.

Huang, R., Wu, Y., 1989. The influence of ENSO on the summer climate change in China and its mechanism. Adv. Atmos. Sci. 6, 21-32.

Jia, G., Rao, Z., Zhang, J., Li, Z., Chen, F., 2013. Tetraether biomarker records from a loess-paleosol sequence in the western Chinese Loess Plateau: Front. Microbial. 4.

Jia, Q., Li, T., Xiong Z. Chang F., 2015. Foraminiferal carbon and oxygen isotope composition characteristics and their paleoceanographic implications in the north margin of the western Pacific warm pool over the past about 700,000 years. Chinese J. Quatern. Res. 35, 401-410. In Chinese, with English abstract.

Jiang, D., Lang, X., Tian, Z., Guo, D., 2011. Last glacial maximum climate over China from PMIP simulations. Palaeogeogr. Palaeocl. 309, 347-357.

Kalnay, E., Kanamitsu, M., Kistler, R., Collins, W., Deaven, D., Gandin, L., Iredell, M., Saha, S., White, G., Woollen, J., 1996. The NCEP/NCAR 40-year reanalysis project. B. Am. Meteorol. Soc. 77, 437-471.

Kukla, G., Heller, F., Liu, X., Xu, T., Liu, T., An, Z., 1988. Pleistocene climates in China dated by magnetic susceptibility. Geology 16, 811-814.

Kutzbach, J.E., Guetter, P.J., 1986. The Influence of Changing Orbital Parameters and Surface Boundary Conditions on Climate Simulations for the Past 18 000 Years. J. Atmos. Sci. 43, 1726-1759.

Kutzbach, J.E., Liu, X., Liu, Z., Chen, G., 2008. Simulation of the evolutionary response of global summer monsoons to orbital forcing over the past 280,000 years. Clim. Dynam. 30, 567-579.

Lea, D.W., Pak, D.K., Spero, H.J., 2000. Climate Impact of Late Quaternary Equatorial Pacific Sea Surface Temperature Variations. Science 289, 1719.

Lisiecki, L.E., Raymo, M.E., 2005. A Pliocene-Pleistocene stack of 57 globally distributed benthic $\delta^{18}O$ records. Paleoceanography 20, 1003.

Liu, W., Huang, Y., An, Z., Clemens, S. C., Li, L., Prell, W. L., Ning, Y., 2005. Summer monsoon intensity controls C4/C3 plant abundance during the last 35 ka in the Chinese

Loess Plateau: Carbon isotope evidence from bulk organic matter and individual leaf waxes. Palaeogeogr. Palaeocl. 220, 243-254.

Liu, Y., Henderson, G.M., Hu, C., Mason, A.J., Charnley, N., Johnson, K.R., Xie, S., 2013. Links between the East Asian monsoon and North Atlantic climate during the 8,200 year event: Nat. Geosci. 6, 117-120.

Liu, Z., Wen, X., Brady, E.C., Otto-Bliesner, B., Yu, G., Lu, H., Cheng, H., Wang, Y., Zheng, W., Ding, Y., 2014. Chinese cave records and the East Asia Summer Monsoon. Quat. Sci. Rev. 83, 115-128.

Lu, H., Wu, N., Liu, K., Jiang, H., Liu, T., 2007. Phytoliths as quantitative indicators for the reconstruction of past environmental conditions in China II: palaeoenvironmental reconstruction in the Loess Plateau. Quat. Sci. Rev. 26, 759-772.

Lu, H., Yi, S., Liu, Z., Mason, J.A., Jiang, D., Cheng, J., Stevens, T., Xu, Z., Zhang, E., Jin, L., 2013. Variation of East Asian monsoon precipitation during the past 21 k.y. and potential CO_2 forcing. Geology 41, 1023-1026.

Manabe, S., Broccoli, A.J., 1990. Mountains and Arid Climates of Middle Latitudes. Science 247, 192.

McManus, J.F., Oppo, D.W., Cullen, J.L., 1999. A 0.5-million-year record of millennial-scale climate variability in the North Atlantic. Science 283, 971-975.

McManus, J.F., Francois, R., Gherardi, J.-M., Keigwin, L. D., Brown-Leger, S., 2004. Collapse and rapid linked to deglacial climate changes. Nature 428, 834-837.

Meckler, A.N., Clarkson, M.O., Cobb, K.M., Sodemann, H., Adkins, J.F., 2012. Interglacial hydroclimate in the tropical West Pacific through the Late Pleistocene. Science 336, 1301-1304.

Meehl, G.A., Hu, A. 2006. Megadroughts in the Indian monsoon region and southwest North America and a mechanism for associated multidecadal Pacific sea surface temperature anomalies. J. Climate 19, 1605-1623.

O'Leary, M.H., 1988. Carbon isotopes in photosynthesis. Biosciences 38, 328–336.

Overpeck, J. T., 2013. Climate Science: The challenge of hot drought. Nature 503, 350-351.

Paillard, D., Labeyrie, L., Yiou, P., 2013. Macintosh Program performs time- series analysis. Eos Trans. AGU 77, 379-379.

Pausata, F.S.R., Battisti, D.S., Nisancioglu, K.H., Bitz, C.M., 2011. Chinese stalagmite $\delta^{18}O$ controlled by changes in the Indian monsoon during a simulated Heinrich event. Nat. Geosci. 4, 474-480.

Pena, L.D., Cacho, I., Ferretti, P., Hall, M.A., 2008. El Niño–Southern Oscillation–like variability during glacial terminations and interlatitudinal teleconnections. Paleoceanography 23(3).

Peterse, F., Prins, M.A., Beets, C.J., Troelstra, S.R., Zheng, H., Gu, Z., Schouten, S., Sinninghe Damsté, J.S., 2011. Decoupled warming and monsoon precipitation in East Asia over the last deglaciation. Earth Planet. Sci. Lett. 301, 256-264.

Peterse, F., Meer, J., Schouten, S., Weijers, J.W.H., Fierer, N., Jackson, R.B., Kim, J.H., Sinninghe Damsté, J.S., 2012. Revised calibration of the MBT-CBT paleotemperature proxy based on branched tetraether membrane lipids in surface soils. Geochim. Cosmochim. Acta 96, 215–229.

Peterse, F., Martínez-García, A., Zhou, B., Beets, C.J., Prins, M.A., Zheng, H., Eglinton, T.I., 2014. Molecular records of continental air temperature and monsoon precipitation variability in East Asia spanning the past 130,000 years. Quatern. Sci. Rev. 83, 76-82.

Petit, J., Jouzel, J., Raynaud, D., Barkov, N.I., Barnola, J., Basile, I., Bender, M., Chappellaz, J., Davis, M., Delaygue, G., 1999. Climate and atmospheric history of the past 420,000 years from the Vostok ice core, Antarctica. Nature 399, 429-436.

Porter, S.C., An, Z., 1995. Correlation between climate events in the North Atlantic and China during the last glaciations. Nature 375, 305-308.

Schouten, S., Hopmans, E.C., Sinninghe Damsté, J.S., 2013. The organic geochemistry of glycerol dialkyl glycerol tetraether lipids: A review. Org. Geochem. 54, 19-61.

Sun, J., Lü, T., Zhang, Z., Wang, X., Liu, W., 2011. Stepwise expansions of C4 biomass and enhanced seasonal precipitation and regional aridity during the Quaternary on the southern Chinese Loess Plateau. Quatern. Sci. Rev. 34, 57-65.

Sun, Y., Chen, J., Clemens, S.C., Liu, Q., Ji, J., Tada, R., 2006. East Asian monsoon variability over the last seven glacial cycles recorded by a loess sequence from the northwestern Chinese Loess Plateau. Geochem. Geophys. Geosyst. 7, 97-112.

Sun, Y., Clemens, S.C., Morrill, C., Lin, X., Wang, X., An, Z., 2012. Influence of Atlantic meridional overturning circulation on the East Asian winter monsoon. Nat. Geosci. 5, 46-49.

Sun, Y., Kutzbach, J., An, Z., Clemens, S., Liu, Z., Liu, W., Liu, X., Shi, Z., Zheng, W., Liang, L., 2015. Astronomical and glacial forcing of East Asian summer monsoon variability. Quat. Sci. Rev. 115, 132-142.

Thomas, E.K., Clemens, S.C., Sun, Y., Prell, W.L., Huang, Y., Gao, L., Loomis, S., Chen, G., Liu, Z., 2016. Heterodynes dominate precipitation isotopes in the East Asian monsoon region, reflecting interaction of multiple climate factors. Earth Planet. Sci. Lett. 455, 196-206.

Thomas, E.K., Clemens, S.C., Sun, Y., Huang, Y., Prell, W., Chen, G., Liu, Z., Loomis, S., 2017. Midlatitude land surface temperature impacts the timing and structure of glacial maxima. Geophys. Res. Lett. 44, 984-992.

Wang, H., Liu, W., Zhang, C.L., Liu, Z., He, Y., 2013. Branched and isoprenoid tetraether (BIT) index traces water content along two marsh-soil transects surrounding Lake Qinghai: Implications for paleo-humidity variation. Org. Geochem. 59, 75-81.

Wang, Y., Cheng, H., Edwards, R.L., Kong, X., Shao, X., Chen, S., Wu, J., Jiang, X., Wang, X., An, Z., 2008. Millennial-and orbital-scale changes in the East Asian monsoon over the past 224,000 years. Nature 451, 1090-1093.

Weber, S.L., Tuenter, E., 2011. The impact of varying ice sheets and greenhouse gases on the intensity and timing of boreal summer monsoons. Quat. Sci. Rev. 30, 469-479.

Webster, P.J., Magana, V.O., Palmer, T.N., Shukla, J., Tomas, R.A., Yanai, M.U., Yasunari, T., 1998. Monsoons: Processes, predictability, and the prospects for prediction. J. Geophys. Res. 103, 14451-14510.

Weijers, J.W., Schouten, S., van den Donker, J.C., Hopmans, E.C., Sinninghe Damsté, J.S., 2007. Environmental controls on bacterial tetraether membrane lipid distribution in soils. Geochim. Cosmochim. Acta 71, 703-713.

Xiao, Z., Sun, J., Li C., 2000. Influence of the Indian Ocean SSTA on Asian Climate during an ENSO Period. Chinese J Atmos. Sci. 24, 461-468. In Chinese, with English abstract.

Xie, S., Pancost, R.D., Chen, L., Evershed, R.P., Yang, H., Zhang, K., Huang, J., Xu, Y., 2012. Microbial lipid records of highly alkaline deposits and enhanced aridity associated with significant uplift of the Tibetan Plateau in the Late Miocene. Geology 40, 291-294.

Yanase, W., Abe-Ouchi, A., 2007. The LGM surface climate and atmospheric circulation over East Asia and the North Pacific in the PMIP2 coupled model simulations. Clim. Past 3, 551-554.

Yancheva, G., Nowaczyk, N.R., Mingram, J., Dulski, P., Schettler, G., Negendank, J.F., Liu, J., Sigman, D.M., Peterson, L.C., Haug, G.H., 2007. Influence of the intertropical convergence zone on the East Asian monsoon. Nature 445, 74-7.

Yang, H., Lü, X., Ding, W., Lei, Y., Dang, X., Xie, S., 2015. The 6-methyl branched tetraethers significantly affect the performance of the methylation index (MBT′) in soils from an altitudinal transect at Mount Shennongjia. Org. Geochem. 82, 42-53.

Yang, H., Pancost, R.D., Dang, X., Zhou, X., Evershed, R.P., Xiao, G., Tang, C., Gao, L., Guo, Z., Xie, S., 2014. Correlations between microbial tetraether lipids and environmental variables in Chinese soils: Optimizing the paleo-reconstructions in semi-arid and arid regions. Geochim. Cosmochim. Acta 126, 49-69.

Zech, M., Zech, R., Glaser, B., 2007. A 240,000-year stable carbon and nitrogen isotope record from a loess-like palaeosol sequence in the Tumara Valley, Northeast Siberia. Chem. Geol. 242, 307–318.

Zhang, H., Griffiths, M.L., Huang, J., Cai, Y., Wang, C., Zhang, F., Cheng, H., Ning, Y., Hu, C., Xie, S., 2016. Antarctic link with East Asian summer monsoon variability during the Heinrich Stadial–Bølling interstadial transition. Earth Planet. Sci. Lett. 453, 243-251.

Zhang, P., Cheng, H., Edwards, R.L., Chen, F., Wang, Y., Yang, X., Liu, J., Tan, M., Wang, X., Liu, J., 2008. A test of climate, sun, and culture relationships from an 1810-year Chinese cave record. Science 322, 940-942.

Zhang, Z., Zhao, M., Lu, H., Faiia, A. M., 2003. Lower temperature as the main cause of C4 plant declines during the glacial periods on the Chinese Loess Plateau. Earth Planet. Sci. Lett. 214, 467-481.

Thesis

Zan, J., 2010. Loess on west Kunlun Moutains and aridification of Asian inland [Ph.D. thesis]: Lanzhou, Lanzhou University, 140 p, in Chinese.

FIGURES

Fig.1

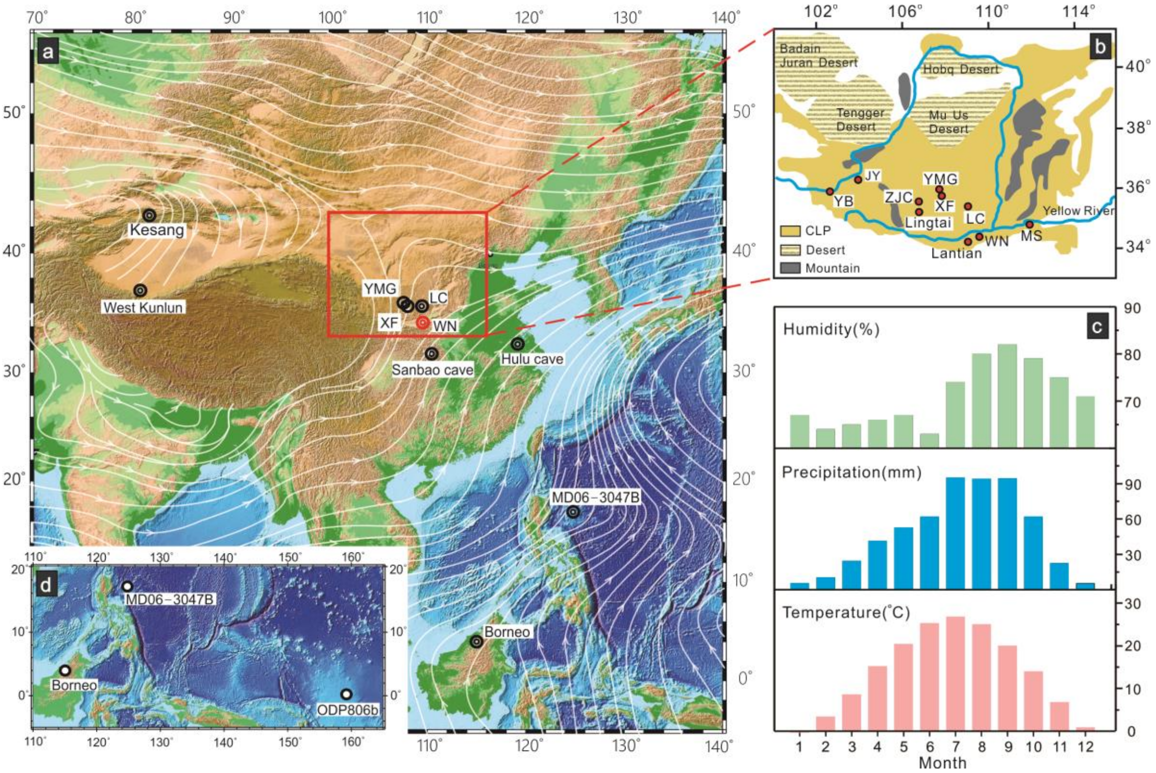

Fig. 1. The locality (a, b) and modern climatology (c) of the Weinan section and the sites mentioned in the text, as well as the averaged atmospheric flow fields at 700 hPa isobaric in summer (JJA) from 1971 to 2000 (a, Kalnay et al., 1996; An et al., 2012). The location of loess-paleosol sections mentioned in the text (a, b) include: WN (Weinan section, this study and Thomas et al., 2016, 2017; 34°21′ N; 109°32′E), MS (Mangshan, Peterse et al., 2011, 2014; 34°57′N, 113°22′E), Lantian (Gao et al., 2012; 34°12′N, 109°12′E), YB (Yuanbao, Jia et al., 2013; 103°09′N, 35°38′E), XF (Xifeng, 35°45’N, 107°49’E, Guo et al., 2009), YMG (Yimaguan,35°55′N, 107°37′E, Hao et al., 2012), LC (Luochuan, 35°43′N, 109°25′E, Hao et al., 2012), Lingtai (35°04′N, 107°39′E,Sun et al., 2006), ZJC (Zhaojiachuan, 35°45′N, 107°49′E, Sun et al., 2006), JY (Jingyuan, 36°21′N, 104°4′E,Sun et al., 2006) and west Kunlun loess site (37°0′ N; 80°81′E, Zan, 2010). Chinese caves mentioned in the text include: Kesang cave (42°87′ N; 81°75′E, Cheng et al., 2012) , Sanbao cave (110°26′E, 31°40′N, Wang et al., 2008), and Hulu Cave (32°30′N, 119°10′E, Cheng et al., 2009, 2016). Also shown is location of speleothem records from Borneo (4°N, 115°E, Meckler et al., 2012; Carolin et al., 2016). The location of western Pacific MD06-3047B core (17°00′N; 124°48′E,

Jia et al., 2015) and ODP806b (0°11′N, 159°13′E, Lea, 2000) was shown in subfigure d.

Fig.2

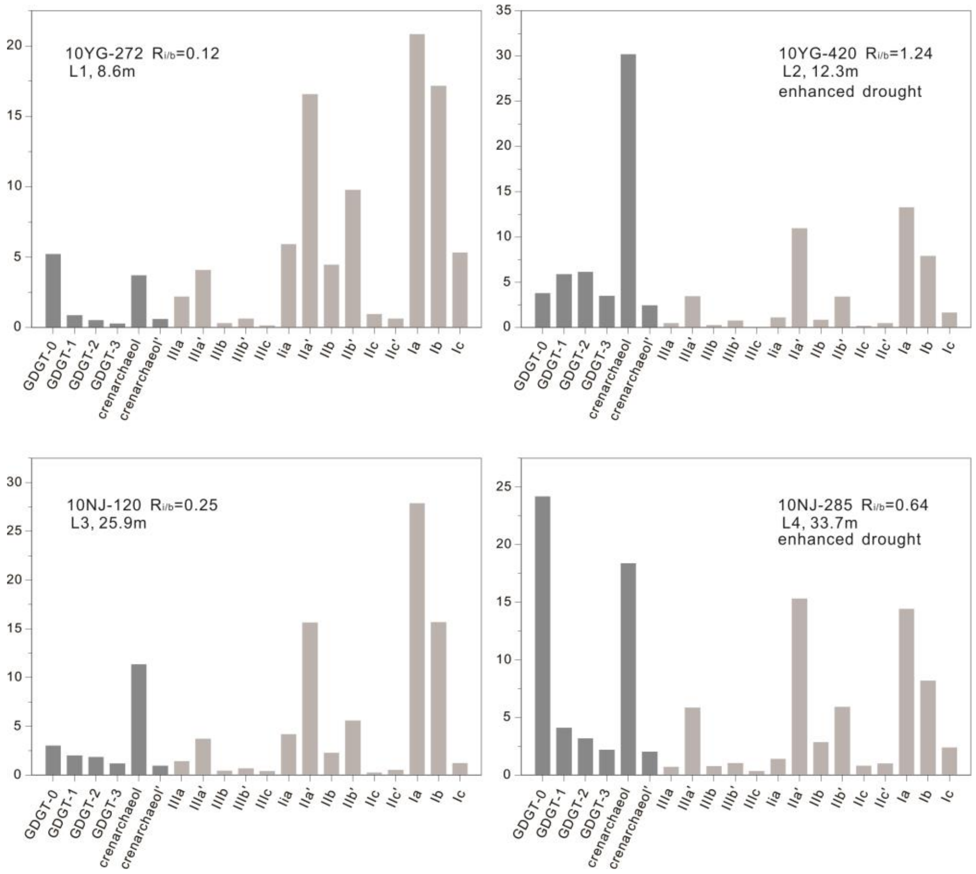

Fig. 2. The GDGTs distributions of four typical samples with completely different $R_{i/b}$ values diagnostic of different dry conditions. The roman numerals denote the corresponding GDGT components shown in supplemental data Fig. S1.

Fig.3

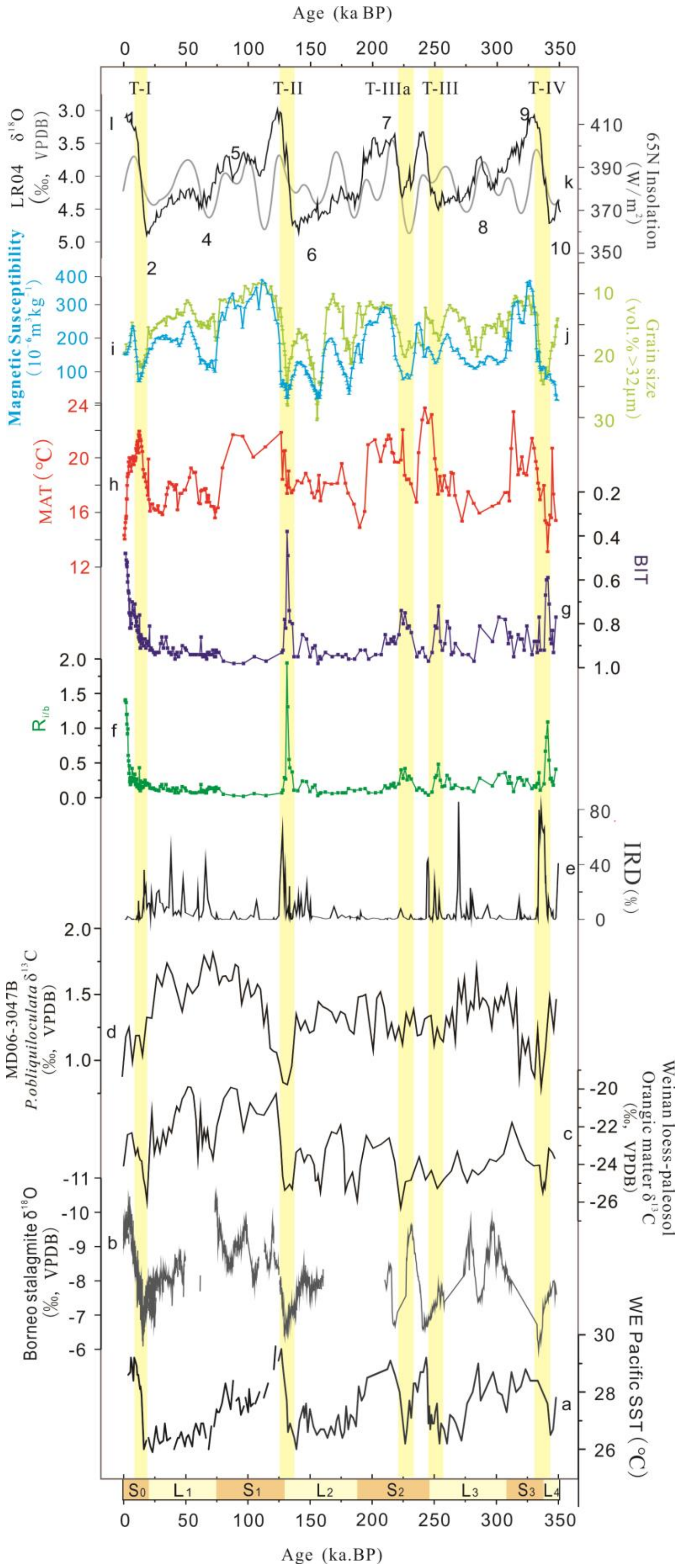

Fig. 3. Variations of GDGT parameters compared with other records. (a) marine sediment

Mg/Ca SST reconstructions from WEP site ODP 806b (Lea, 2000); (b) Speleothem $\delta^{18}O$ records from Borneo (Meckler et al., 2012; Carolin et al., 2013,2016); (c) $\delta^{13}C$ of bulk soil organic matter of Weinan loess-paleosol (Sun et al., 2011); (d) $\delta^{13}C$ of *P. obliquiloculata* in western Pacific warm pool (Jia et al., 2015); (e) ice-rafted debris in North Atlantic (McManus et al., 1999); (f) $R_{i/b}$ and (g) BIT in Weinan, indicative of extreme drought events (this study); (h) annual mean atmospheric temperature (MAT) estimated by the MAT-mr calibration based on 5- and 6-methylated brGDGTs (this study, supplementary data, Table S1), (i) magnetic susceptibility, and (j) loess grain size (vol.% >32μm) for the loess-paleosol sequences in Weinan section (this study); (k) benthic foraminifera $\delta^{18}O$ stack (Lisiecki and Raymo, 2005); and (l) the 65°N insolation (Berger et al., 2010). All the colored curves (f, g, h, i, j) are from Weinan section. The highlight yellow bars indicate the termination I, II, IIIa, III and IV denoted by T-I, T-II, T-IIIa, T-III, T-IV, respectively. The lithologic column shows the loess (light brown, L) and paleosol (dark brown, S) layers.

Fig.4

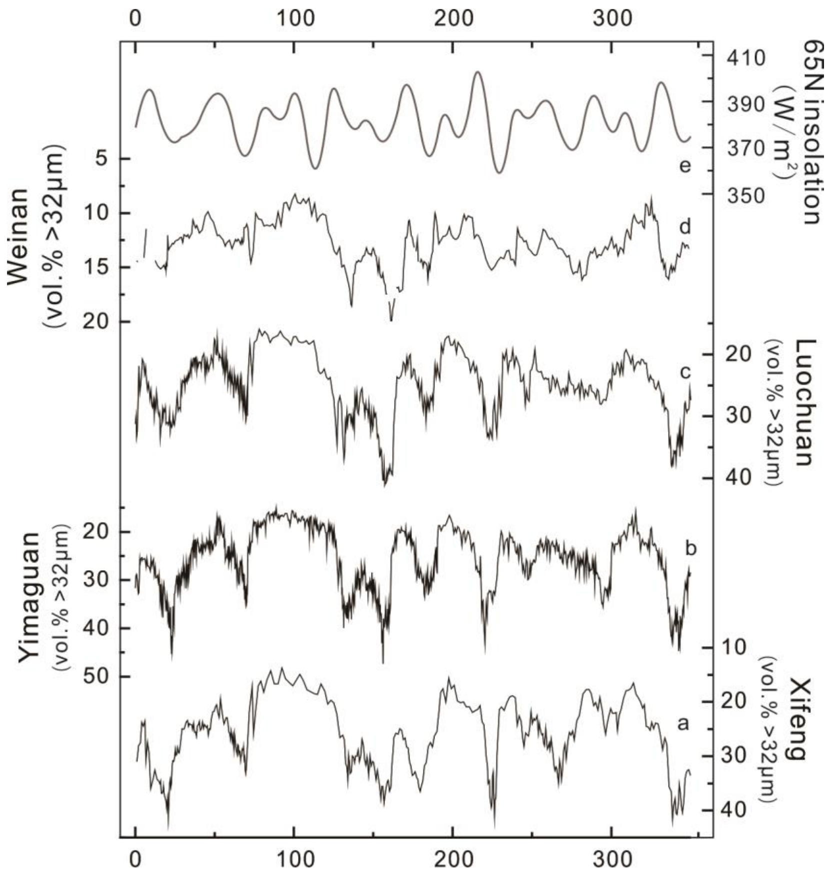

Fig. 4. Grain size (vol.% >32μm) (a, b, c, d) variations in CLP along with the 65°N insolation

(e) (Berger et al., 2010). (a) Xifeng (35°45’N 107°49’E, Guo et al., 2009); (b) Yimaguan (35°55′ N; 107°37′E, Hao et al., 2012); (c) Luochuan (35°43′ N; 109°25′E, Hao et al., 2012); (d) Weinan (34°21′ N; 109°32′E, this study).

Fig.5

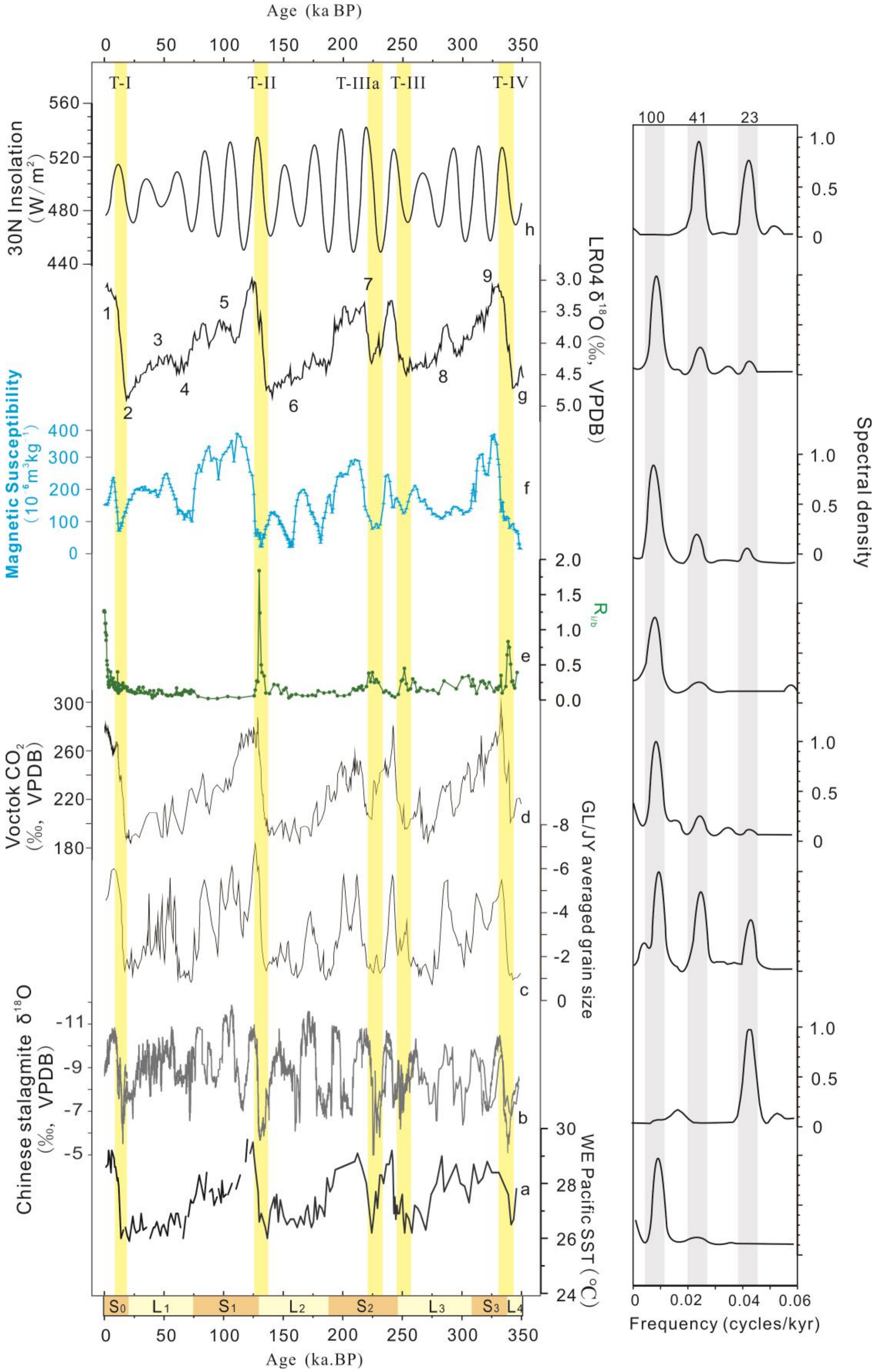

Fig.5 Time series and spectral analysis results of monsoonal proxies. (a) speleothem $\delta^{18}O$ from the Hulu and Sanbao caves (Wang et al., 2008; Cheng et al., 2009); (b) averaged $\delta^{13}C_{IC}$

results of GL/JY sections; (c) CO_2 (Petit et al., 1999); (d) $R_{i/b}$ and (e) magnetic susceptibility from Weinan loess section (this study); (f) benthic $\delta^{18}O$ stack (Lisiecki and Raymo, 2005) and (g) summer insolation (Berger et al., 2010).